Composite Structures 330 (2024) 117846

Contents lists available at ScienceDirect

Composite Structures

journal homepage: www.elsevier.com/locate/compstruct

# High-$T_g$ shape memory polyimide composites with "spot-plane" directional thermally conduction structure based on AlN nanoparticles and acidified graphene

Xiaofei Wang [a,d], Yang He [a], Xinli Xiao [b], Wei Zhao [c], Jinsong Leng [a,*]

[a] National Key Laboratory of Science and Technology on Advanced Composites in Special Environments, Harbin Institute of Technology, Harbin 150080, PR China
[b] MIIT Key Laboratory of Critical Materials Technology for New Energy Conversion and Storage, School of Chemistry and Chemical Engineering, Harbin Institute of Technology, Harbin 150001, PR China
[c] Department of Astronautical Science and Mechanics, Harbin Institute of Technology, Harbin 150001, PR China
[d] Suzhou Research Institute, Harbin Institute of Technology, Suzhou 215100, PR China

ARTICLE INFO

*Keywords:*
High transition temperature
Shape memory polyimide
Acidified graphene
Directional thermally conduction

ABSTRACT

In order to enhance the thermal conduction property and shorten response time of shape memory polyimide (SMPI), "spot-plane" directional thermally conductive acidified graphene/AlN/SMPI composites were prepared, in which AlN nanoparticles were used as "thermal conduction spots" and acidified graphene was used as two-dimensional "thermal conduction planes". The SMPI composite doped with 6 wt% AlN and 0.8 wt% acidified graphene had good heat conducting properties (the in-plane thermal conductivity of 5.90 W $m^{-1}$ $K^{-1}$), excellent mechanical propertied (the tensile strength of 134.5 MPa, and Young's modulus of 3.8 GPa), high shape memory transition temperature (at 419 ℃), and great thermal stability and shape memory properties. Compared with SMPI resin matrix, the response time of the acidified graphene/AlN/SMPI composite was shortened by 140 s, only 20 s, and it can be applied in flexible electronics, intelligent response structures and active deformation structures in high-temperature environment.

## 1. Introduction

Shape memory polymer (SMP) is a kind of smart material with lightweight, high deformation ratio and processability, which actively deforms under external stimuli. The stimuli methods include thermal, light, electricity, magnetism, and solvent, etc. [1–7]. Hu et al. designed a two-way shape-memory cellulose vascular stent, which could realize shape adjustments by mild solutions such as water and alcohol. Ex vivo experiments revealed that the novel vascular stent could support arteria coronaria sinistra, or the left main coronary artery, thus, it made meritorious fundamental contributions to biomaterials science and practical applications [7]. Shape memory switches included amorphous (e.g. the glass transition temperature) or semi-crystalline phases (e.g. the crystallization melting point), supramolecular, photosensitive, and mercapto units, etc. The shape memory effects (SMEs) of SMPs have been developed from the conventional one-way SMEs to two-way, triple and even multiple SMEs [8]. The typical shape memory mechanism is as follows, when the temperature is higher than the shape memory transition temperature ($T_{trans}$), the SMP molecular chain in the soft segment is in a high elastic state, and the SMP is deformed from an original shape to a temporary shape under external force. After that, the SMP is cooled to lower than the $T_{trans}$, and the molecular chain motion is frozen, and the temporary shape is fixed. When the temperature rises to the $T_{trans}$ again, the molecular chain will rearrange under entropy elasticity effect, macroscopically, the SMP returns to its original shape [9]. There are many types of SMPs that have been developed, including shape memory polyimide (SMPI), shape memory polylactic acid, and shape memory polycaprolactone, etc. [10–12]. Specially, SMPI has great shape memory effect, radiation resistance, mechanical properties, and thermal stability, which has bright prospects in sensors, flexible electronics, and aerospace morphing structures, etc. [13]. For example, Yao et al. modified the SMPI with polyoctasiloxane (POSS), which had a strain of up to 247% and a shape recovery ratio of 94.3% [14]. Tan et al. utilized 4,4′-oxydianiline, biphenyltetracarboxylic dianhydride, and 6-chloropurine to produce various copolyimides, specifically, API3 had excellent shape memory performances, and the $T_{trans}$ was 271.1 ℃. After

* Corresponding author.
*E-mail address:* lengjs@hit.edu.cn (J. Leng).

https://doi.org/10.1016/j.compstruct.2023.117846
Received 8 August 2023; Received in revised form 4 December 2023; Accepted 21 December 2023
Available online 23 December 2023

the tensile strain was 358%, the shape recovery ratio was still 100% [15]. In the previous work, we used aromatic heterocyclic diamines and dianhydride to produce SMPI with a $T_{trans}$ of more than 400 ℃, but their engineering applications were limited due to the too long response time, thus, we carried out the modification investigations for high-$T_g$ SMPI.

Generally, the thermal conduction of SMP is important for response speed, which can be improved by doping high heat conduction particles, liking graphene, carbon nanotubes (CNTs), graphdiyne, AlN nanoparticles, and various metal particles [16,17]. When the amounts of particles are little, the thermal conductivity does not increase significantly, due to insufficient contact with heat conduction particles. If the content of the particles overtakes a criticality value, they could form efficient thermal conduction paths in the SMP matrix, thereby enhancing the heat conduction property and response speed [18]. Xiao et al. utilized benzoxazole-containing diamine, hexafluorodianhydride and modified BN (M-BN) nanoparticles to prepare SMPI composite films. Thermal diffusivity of the SMPI composite with 10 wt% M-BN was 0.190 $mm^2/s$, which accelerated the shape recovery process. Although there are many reports on the SMPs enhanced by single thermal conduction particles, few reports on the SMP enhancement of binary particles [19]. Additionally, the interface defects caused by the fillers have high thermal resistance effects, thus, the thermal conduction performances of composites were reduced [20]. The strategies of particles surface modification could strengthen the interaction between fillers and matrices and decrease the interface heat resistance. Because the modified particles could improve the dispersion ability in the matrix and reduce the agglomeration, also increase the possibility to form thermal conduction networks [21,22].

Graphene is a six membered ring plane structure formed by single-layer carbon atoms hybridized with $SP^2$, which is an ideal two-dimensional plane material. Due to its special two-dimensional crystal structure, it has the advantages of high mechanical strength, high electron mobility, and large specific surface area, etc., and the thermal conductivity (TC) is over 6600 W $m^{-1}k^{-1}$ in theory [23]. Graphdiyne (GDY) is a new two-dimensional full-carbon nanomaterial found after graphene and CNTs, and the thermal conductivity value of GDY is about half of graphene. Besides, GDY shows larger specific surface area and lower atom density than that of graphene, thus which might express higher thermal performance in actual applications [24]. However, their interfacial compatibilities with the resin matrix are poor, so, the surfaces need to be modified. The modification methods include physical, chemical and acidification methods [25,26]. Specifically, the acidification method is to open six membered rings of the carbon nanomaterial by oxidation with strong oxidant, so as to generate carboxyl, hydroxyl, and other functional groups [27]. For the composites with randomly distributed particles, the heat energy is transferred in multiple directions, and the energy transfer efficiency is relatively low; when the thermal conductive particles are arranged in a certain direction, the heat energy is transferred along the orientation direction, and the energy transfer efficiency is improved significantly. The surface of acidified carbon nanomaterial contains hydroxyl and carboxyl groups, which could generate positive $H^+$ and negative $OH^-$ charges and improve the directional arrangement performance under the electric field, and enhance the directional thermally conduction property [28].

In this paper, firstly, we acidified the surface of graphene to make it rich in hydroxyl and carboxyl groups; secondly, the acidified graphene and AlN nanoparticles modified with silane coupling agent were mixed evenly with diamine and dianhydride solution to prepare polyamide acid solution. After that, the polyamide acid solution was treated by an electric field. Finally, the solution was placed in a high temperature oven for thermal amination. AlN nanoparticles were as "thermal conduction spots" and acidified graphene was as two-dimensional "thermal conduction planes" to construct "spot-plane" directional thermally conduction structures. Thus, the SMPI composite had good thermal conductivity, fast response, excellent mechanical properties, high thermal stability and high $T_{trans}$, which had bright applications in high-temperature environments, such as space deployable structures (solar panels and derailment sails), high-temperature active deformation structures (re-entry deceleration parachute), and etc.

## 2. Experiment

### 2.1. Materials and reagents

Graphene was from Shenzhen Qihang Technology Co., Ltd. The thickness was 1.0–1.77 nm, the sheet diameter was 10–50 μm, the number of layers was 1–5, the monolayer ratio was more than 30%, and the specific surface area was 360–450 $m^2/g$. Dimethyl sulfoxide solvent (DMSO), 3,3′,4,4′-biphenyltetracarboxylic dianhydride (BPDA), and 5-amino-2-(4-aminophenyl) benzimidazole (DAPBI) were purchased from Shanghai Aladdin Reagent Co., Ltd. The concentrated sulfuric acid ($H_2SO_4$), concentrated nitric acid ($HNO_3$), and ethanol were all from Tianjin Fengchuan Reagent Technology Co., Ltd. Distilled water and AlN nanoparticles (300–500 nm) modified by silane coupling agent KH-550 (named M-AlN) were both from our laboratory.

### 2.2. Acid modification of graphene

According to the literature [29], 0.2 g graphene was put into a beaker, then, 60 mL mixed acid solution with $H_2SO_4$ and $HNO_3$ (volume ratio = 3:1) was added into the beaker, which was placed into 60 ℃ ultrasound equipment for 3 h. After that, the turbid liquid was diluted to neutral by using distilled water, finally, it was dried at 100 ℃ baking oven to obtain acidified graphene, named AG.

### 2.3. Construction of SMPI composite with "spot-plane" directional thermally conduction structure

(I) (I) M-AlN nanoparticles and AG were poured into DMSO, and was sonicated for 30 min, also, DAPBI was dissolved in the mixed solution fully, after that, BPDA was also dissolved in the system, and stirred for 120 h to obtain polyamic acid solution (named PAA). The molar ratio of DAPBI and BPDA was 1:1, the content of M-AlN was 6 wt%, and the contents of AG were 0.2, 0.4, 0.6, 0.8, and 1.0 wt%, respectively.

(II) (II) PAA solution obtained by step (I) was poured on a glass mold, then, a direct current electric field was applied to both ends of the solution. The voltage was 15 V, and the time was 120 s.

(III) (III) The PAA solution obtained by step (II) was put in an oven and went through an imidization process, as a result, the SMPI composite films (named AG/M-AlN/M-SMPI) with "spot-plane" directional thermally conduction structures were produced. The heating processes were as follows: 50 ℃ for 5 h, 80 ℃ for 5 h, 120 ℃ for 2 h, 160 ℃ for 2 h, 200 ℃ for 2 h, 250 ℃ for 2 h, and 300 ℃ for 2 h. The synthesis process and production route were shown in Fig. 1. The composites were named as AG/M-AlN/M-SMPI-0.2, AG/M-AlN/M-SMPI-0.4, AG/M-AlN/M-SMPI-0.6, AG/M-AlN/M-SMPI-0.8, and AG/M-AlN/M-SMPI−1.0, respectively.

### 2.4. Characterization

The functional group structure of graphene, AG, and SMPI composite films were characterized by AVATAR360 FTIR spectrometer, and the range of wavelength was 4000–500 $cm^{-1}$. The absorbance of the graphene and acidified graphene were tested by UV–vis spectrophotometre (METTLER-TOLEDO Corporation, Switzerland), and the range of wavelength was 200–800 nm. Graphene and AG were dispersed in the ethanol solution with a concentration of 0.1 mg/mL. After centrifugation process, the supernatant was used for UV–vis test. The crystallinity of SMPI resin matrix and AG/M-AlN/M-SMPI composites were tested by WAXD (D8, Bruker, Germany). The scanning rate was 8°/ min and the range of scanning angle was 5–80°. Dynamic mechanical performances

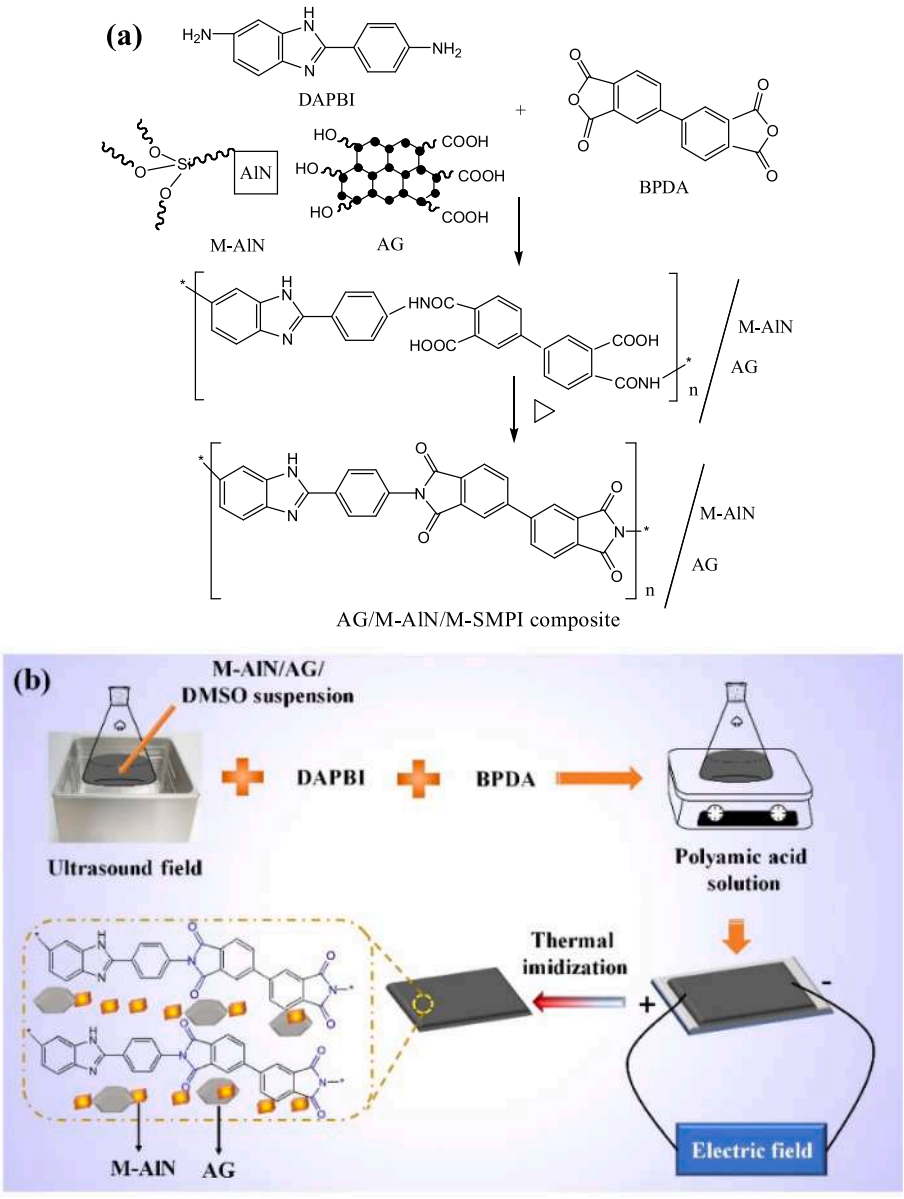


**Fig. 1.** (a, b) Scheme of polycondensation reaction and preparation method of AG/M-AlN/M-SMPI, respectively.

of the composites were tested by DMA analyzer (TA Corporation, USA). The conditions were that $N_2$ atmosphere, the flow rate of 10.00 mL/min, the temperature rise/fall rate of 5 ℃/min, the temperature range of 25–560 ℃, stretch mode, 0.2 % amplitude, and 1 Hz frequency. Thermal stability was characterized by TGA/DSC1 (METTLER-TOLEDO Corporation, Switzerland). The heating process was from 25 ℃ to 800 ℃, $N_2$ atmosphere, the heating rate was 10 ℃/min, and the weight was 5–10 mg. The mechanical properties of the composites were characterized by tensile testing machine (Zwick, Germany), and the dimensions were based on the standard GB/T528-2009, and the tensile speed was 5 mm/min. SEM (JEM-1200, JEOL Company, Japan) was utilized to observe the directional arrangement of AG and the dispersion status of M-AlN and AG in the SMPI resin matrix. Laser thermal conductivity meter (NETZSCH LFA 467, Germany) was utilized to characterize thermally conductive properties of the composites. The characterization of shape memory property was as follows: Firstly, the composite was put on a $T_g$ + 30 ℃ heating platform, and it was shaped into 180° by external force. After that, it was put in 25 ℃ environment for 5 min to obtain a temporary shape. Finally, it was heated to $T_g$ + 30 ℃ again to recover the original shape. Besides, the quantitative shape memory property was tested by DMA. The steps were that: The composite was heated up to $T_g$ + 30 ℃ and was stretched from strain $\varepsilon_0$ to $\varepsilon_0 + \Delta L$ under a certain stress. After that, it was cooled to 250 °C in $N_2$ environment, and the loaded stress was taken away, at the same time, the strain was become to $\varepsilon_0 + \Delta L'$. Finally, it was heated to $T_g$ + 30 °C again to recover the strain $\varepsilon_{rec}$.

The equations of shape fixation ratio ($R_f$) and recovery ratio ($R_r$) were as follows:

$$R_f = \frac{\varepsilon_0 + \Delta L'}{\varepsilon_0 + \Delta L} \times 100\%$$

$$R_r = \frac{\varepsilon_{rec}}{\varepsilon_0 + \Delta L'} \times 100\% \quad (2)$$

## 3. Results and discussion

### 3.1. Molecular structures of graphene, acidified graphene, and AG/M-AlN/M-SMPI

The infrared spectra of graphene and acidified graphene were shown

in Fig. 2a, compared with graphene, the spectrum of acidified graphene had changed significantly. Specifically, the stretching vibration absorption peaks of –OH bond and C=O bond are at 3354 $cm^{-1}$ and 1728 $cm^{-1}$, respectively, also, the bending vibration peak of the carbon oxygen bond in C-O–H and C–O–C bonds is at 1028 $cm^{-1}$, which illustrates that the –COOH group has been successfully introduced into graphene after acidification modification. Additionally, AG has absorption peak at 1643 $cm^{-1}$, which is deformation vibration peak of –OH bond and stretching vibration peak of undamaged conjugated C=C bond. Therefore, a large number of –OH and –COOH bonds were introduced on the graphene surface after acidification treatment. Afterwards, we tested the absorbance of graphene and AG, the results were shown in Fig. 2b. The absorbances of graphene and AG suspension are 0.04 A and 0.16 A, respectively, indicating that the dispersion stability of AG in ethanol solution is significantly improved. In addition, 251 nm is the absorption peak of acidified graphene, which is relevant to the π–π transition of aromatic C–C bond.

The infrared spectra of SMPI composites with different acidified graphene contents were shown in Fig. 2c. The ranges of 1347–1367 $cm^{-1}$ and 1699–1715 $cm^{-1}$ are the characteristic absorption peaks of C-N bond and C=O bond, respectively. As the content of AG increasing, both of them moved to lower wavelength position, because the hydroxyl and carboxyl groups in the AG and the imine groups in the matrix resin formed intermolecular hydrogen bonding. Thus, acidified graphene can be well combined with the organic matrix to increase the compatibility.

WAXD was utilized to characterize the crystalline properties of the composites, as shown in Fig. 2d. It illustrated that as the content of AG increasing, 2$\theta$ (=23.4°) diffraction peak intensity of the composite was increased obviously, indicating that the crystallinity was improved. On one hand, the molecular chains of the SMPI resin matrix were arranged orderly and stacked closely; on the other hand, AG owned unique two-dimensional lamellar structure and could be directional arranged by electric field, which made the planar molecular chains and the two-dimensional AG fillers interpenetrate with each other. Besides, AG promoted the regular arrangement of the molecular chains and improved the crystallinity of the films.

### 3.2. Thermodynamic and mechanical performances of AG/M-AlN/M-SMPI

The storage moduli ($E'$) of AG/M-AlN/M-SMPI-0.2, -0.4, -0.6, -0.8, and −1.0 at room temperature were 2258 MPa, 2944 MPa, 3586 MPa, 3672 MPa, and 3811 MPa, respectively, as shown in Fig. 3a. This was because AG contained abundant hydroxyl and carboxyl groups, and there was great hydrogen bonding interaction between AG and SMPI molecular chains, which increased the rigidity of the polymer chains segments and made the storage modulus increase continuously. With the AG level increasing, the filler networks were formed rapidly, so that the storage modulus had a rapid increase. However, when the content of AG was from 0.6 wt% to 1 wt%, the modulus difference was relatively small, because the filler networks had been established, and the particles began to agglomerate. Thus, the impact of AG on the storage modulus was reduced.

In the process of the temperature rising to 450 ℃, the storage

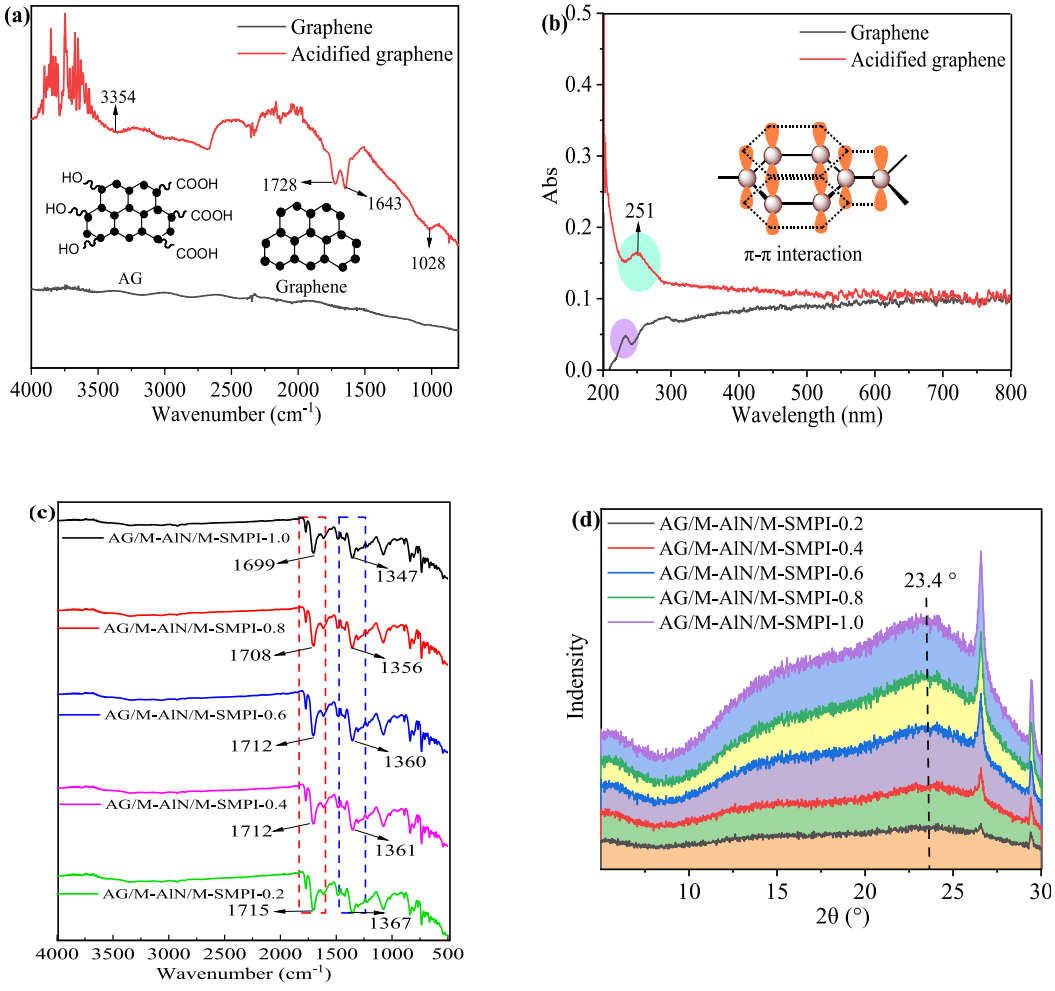


**Fig. 2.** (a, b) The FTIR and UV–vis spectra of graphene and acidified graphene, respectively. (c, d) The FTIR and WAXD spectra of AG/M-AlN/M-SMPI, respectively.

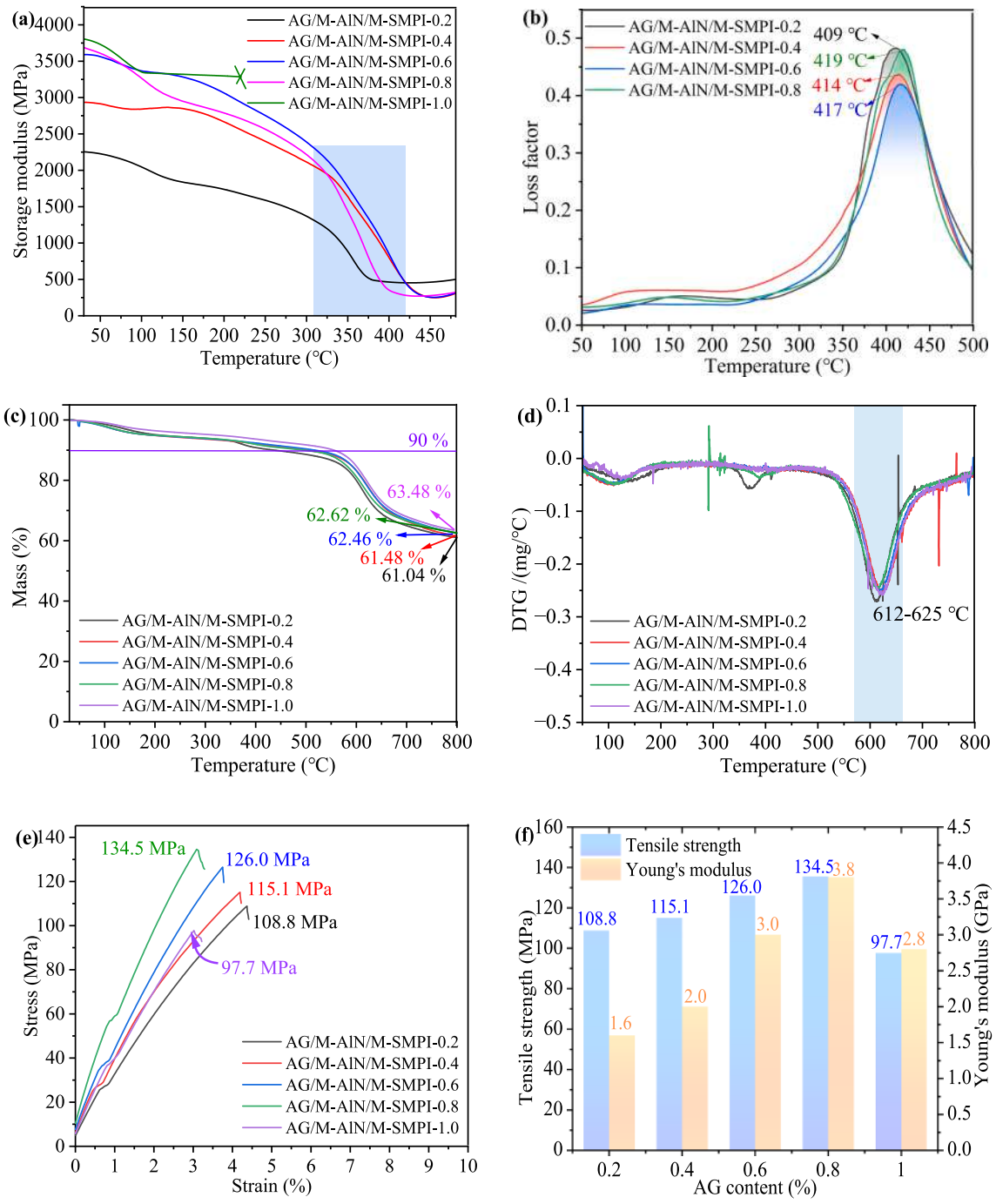


**Fig. 3.** (a, b) The $E'$ and tan$\delta$ curves of AG/M-AlN/M-SMPI. (c, d) TGA and DTG results of AG/M-AlN/M-SMPI. (e, f) Stress–strain curves and mechanical properties of AG/M-AlN/M-SMPI, respectively.

modulus of the composites decreased seriously, and the maximum reduction area was in the range of 350–450 ℃, which was the glass transition range. In addition, the $E'$ curve of AG/M-AlN/M-SMPI−1.0 was broken at 218 ℃, so, the subsequent data cannot be obtained. The loss factor (tan$\delta$) peaks in Fig. 3b were sharp in the range of 380–450 ℃, and the peak positions were between 409 and 419 ℃, thus, the $T_g$ of AG/M-AlN/M-SMPI-0.2, -0.4, -0.6, and -0.8 were 409 ℃, 414 ℃, 417 ℃, and 419 ℃, successively, which also the shape memory transition temperature. As the level of AG raising, the $T_g$ of the composites increased gradually, because the more the AG filled, the stronger the hindrance to the molecular chain motion was, and the more difficult motion of the chain segments became. As a result, the material required a higher temperature to actuate the molecular chains motion.

TGA curves (Fig. 3c) decreased very slowly below 560 ℃, and it illustrated that the mass loss of the AG/M-AlN/M-SMPI composites was extraordinary little in this temperature range, which was the evaporation of small molecules, unreacted monomer molecules, water, and solvent molecules in the composite. 10% mass loss of AG/M-AlN/M-SMPI-0.2, -0.4, -0.6, -0.8 and −1.0 were at 447 ℃, 514 ℃, 524 ℃, 510 ℃ and 558 ℃, successively. In the range of 560–700 ℃, the AG/M-AlN/M-SMPI composites were decomposed rapidly. DTG curves (Fig. 3d) showed that the composites had small peaks at about 120 ℃, which was the volatilization of water in the resin matrix, and then there were small peaks at about 390 ℃, which was the decomposition of small

molecules in the matrix. The maximum decomposition rate temperature appeared between 612 and 625 ℃, it was mainly due to the rapid decomposition of aromatic rings, aromatic heterocycles, and imide rings on the molecular main chains. While the temperature was up to 800 ℃, the residual amounts of the composites were still more than 50%, among them, the residual amount of AG/M-AlN/M-SMPI-0.2, -0.4, -0.6, -0.8, and −1.0 at 800 ℃ was 61.04%, 61.48%, 62.46%, 62.62%, and 63.48%, respectively. As the content of AG increasing, the residual amounts at 800 ℃ were more and more, which showed that AG can improve the thermal stability of the composites. The 5% mass loss of AG/M-AlN/M-SMPI-0.8 and AG/M-AlN/M-SMPI−1.0 were 450 ℃ and 457 ℃, respectively, which was higher than $T_g$, and the residual amount at 800 ℃ exceeded 62.5%, so, both of them had better thermal stability.

In Fig. 3e and f, the mechanical properties of the SMPI composites enhanced first and then reduced with the level of AG increasing. On one hand, acidified graphene filled the gaps generated by AlN nanoparticles and decreased the stress concentration points, so that the stress was distributed uniformly in the matrix. On the other hand, the surface of AG was rich in hydroxyl and carboxyl groups, which could form hydrogen bonds with polyimide molecular chains and improve the tensile strength and Young's modulus, specially, AG/M-AlN/M-SMPI-0.8 had the greatest mechanical properties. However, as the AG content continuous increasing to 1.0 wt%, the tensile strength was decreased, because AG and AlN particles had agglomeration in the resin matrix and damaged the molecular chains structural regularity, generating defects and stress concentration points. It should be noted that when the AG level was 1.0 wt%, the storage modulus and Young's modulus showed different trends. At this time, AG particles had severe agglomeration in the resin matrix, which led to uneven internal stress shrinkage during the thermal imidization process, resulting in the poor film-forming performance, macroscopically, AG/M-AlN/M-SMPI−1.0 composite film was uneven and irregular. And the uneven sample led to different results for the DMA and tensile testing.

### 3.3. Microstructure and thermal conductivity of AG/M-AlN/M-SMPI

The microstructures of AG/M-AlN/M-SMPI composites were characterized by SEM-EDS, including the directional arrangement of the AG in the SMPI matrix and the "spot-plane" position between AlN nanoparticles and two-dimensional AG sheets. In the Fig. 4a (A), the bright part of the cubic shape was AlN nanoparticles, but due to less acidified graphene quantity, it cannot form continuous conductive paths under electric fields, so, the orderly arranged AG sheets were not observed. Fig. 4a (B–E) were illustrated that AG sheets were arranged along the vertical direction, because the surface of AG contained a lot of hydroxyl and carboxyl groups, which generated positive $H^+$ and negative $OH^-$

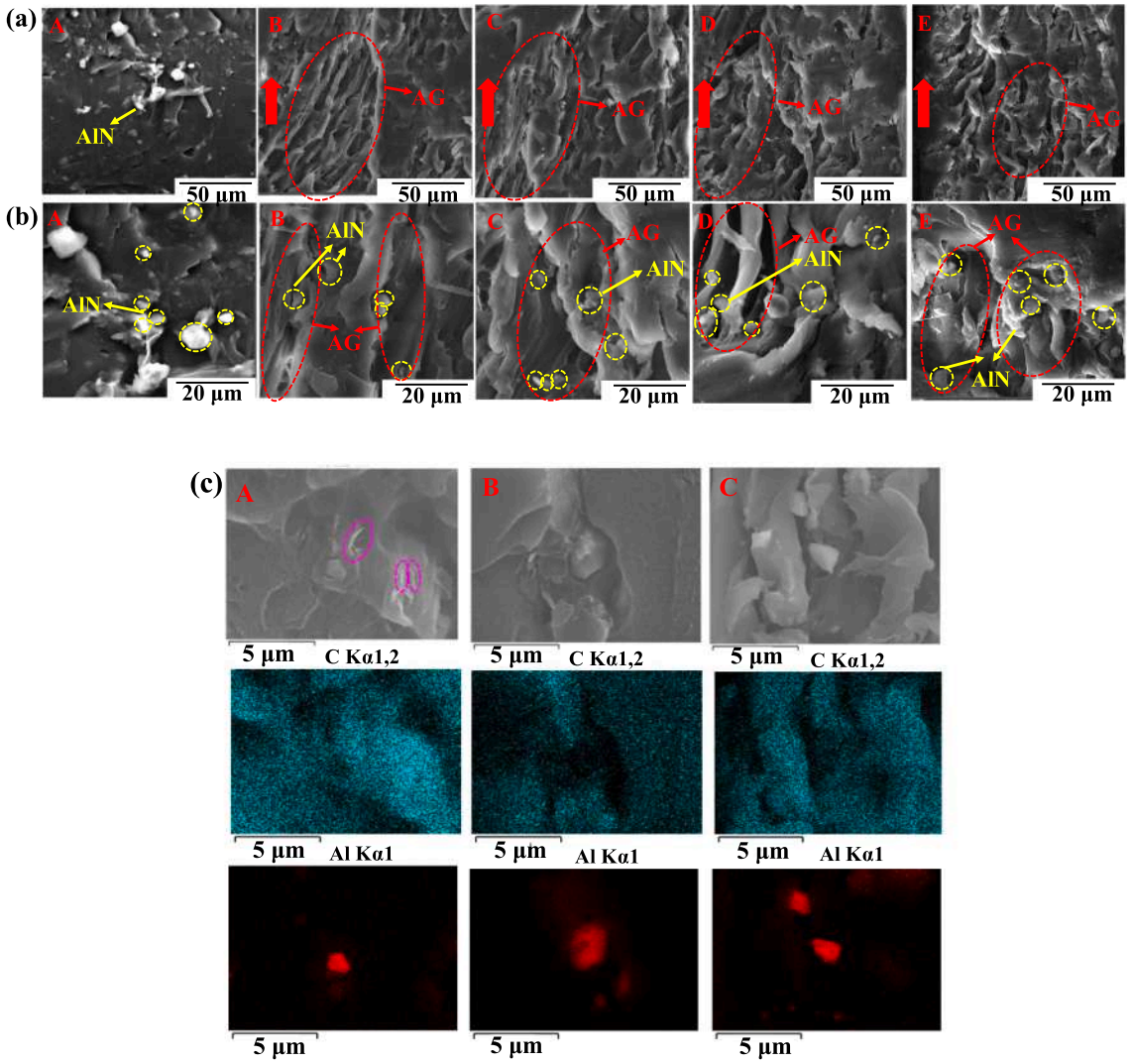


**Fig. 4.** (a, b) SEM images of AG/M-AlN/M-SMPI-0.2, -0.4, -0.6, -0.8, and −1.0 composites, successively. (c) SEM-EDS images of AG/M-AlN/M-SMPI-0.4, -0.6, and -0.8 composites, successively.

charges and was directionally arranged under electric field effects [28].

In Fig. 4b, the yellow and red circles contained AlN nanoparticles and acidified graphene, respectively, and in Fig. 4b (B-D), nano-AlN was evenly dispersed between AG sheets. For further observe their distribution, EDS was utilized to determine the elements of AG/M-AlN/M-SMPI-0.4, -0.6, and -0.8 composites. As shown in Fig. 4c, SEM-EDS images showed the position and distribution of Al element, proving the presence of AlN nanoparticles in the resin matrix. Additionally, it can be seen that AG and AlN were in contact with each other, and the image of C element showed a vertical direction, which further verified the "spot-plane" oriented particles structure. It should be noted that in Fig. 4b, the red circle only marked the location of AG, and it contained AG and resin matrix, not all of AG. Furthermore, the image was not a single graphene, but much AG agglomeration. Multiple single graphene lamellar structures could be observed in Fig. 4c (A), and the clear image was shown in Supporting Information (SI), Scheme 1. The purple circle showed a single graphene lamellar structure, and the dimension was 1–2 nm.

Based on the previous work [30], the in-plane thermal conductivity (TC) of SMPI composite with 6 wt% M-AlN nanoparticles was 5.15 W $m^{-1}K^{-1}$, and the out-of-plane TC was 0.18 W $m^{-1}K^{-1}$ (The relationship between the thermal conductivities and AlN contents was shown in SI, Scheme 2). Fig. 5a illustrated that the thermal conductivity of AG/M-AlN/M-SMPI composites rose continuously with the AG level increasing. Among them, the in-plane and out-of-plane TC of AG/M-AlN/M-SMPI-0.8 were 5.90 W $m^{-1}K^{-1}$ and 0.25 W $m^{-1}K^{-1}$, which was increased by 15% and 38% compared with the SMPI composite with 6 wt% M-AlN, and was increased by 88% and 92% compared with the SMPI resin matrix, respectively. Besides, compared with other modified graphene/PI composites [31–36] in Fig. 5b, the TC of the acidified graphene/AlN/SMPI composites we prepared was very high. The thermal conduction mechanism was shown in Fig. 5c. Acidified graphene was a two-dimensional lamellar structure, which could be arranged directionally under the effect of electric field and form orderly parallel arrangement structure. As the "thermal conduction planes", AG connected the nano "thermal conduction spots" and made up the gaps between M-AlN particles, and they were stacking with each other, which could construct consecutive heat conduction networking paths together and reduce the interface heat resistance greatly [37], so, the TC rose continuously.

### 3.4. Shape memory performances of AG/M-AlN/M-SMPI

From the above tests results, it can be concluded that when the acidified graphene level was 0.8 wt%, the composite film had good comprehensive performance. Therefore, we choose AG/M-AlN/M-SMPI-0.8 as an example to verify the shape memory performance. Firstly, the sample was heated to over the $T_{trans}$, i.e. 449 ℃, and then shaped under external force, including bending 90°, 180°, and wavy shape. After that, the temperature was reduced to the 25 ℃, and the temporary shape was obtained, as shown in Fig. 6a-c. When heated over $T_{trans}$ again, the temporary shape could completely return to its original shape. Among them, the shape recovery time of 90° sample was 8 s (SI, video 1), the shape recovery time of 180° sample was 20 s (SI, video 2), compared with SMPI resin matrix [38] (SI, Scheme 3), the response time was shortened by 140 s. Also, the wavy shape recovery only took 12 s (SI, video 3). AG/M-AlN/M-SMPI-0.8 had 89% shape fixation ratio and 96% shape recovery ratio through thermal mechanical cycle test in Fig. 6d, by contrast, SMPI resin matrix had 84.5% shape fixation ratio and 96% shape recovery ratio [38] (SI, Scheme 4). Thus, AG and AlN fillers had little impact on the shape fixation ratio and recovery ratio of the SMPI composites, but could dramatically shorten the shape recovery time and solve the problem of long response time for high-temperature intelligent materials, providing supports for space deployable structures (solar panels and deorbit sails), high-temperature active deformation structures (re-entry speed reducers), and etc. For example, the reliable locking structure on Venus or Mercury detectors can lock the mechanism when the temperature is lower than the $T_{trans}$, after that, the locking structure can deploy the predesigned shape autonomously when the temperature is higher than the $T_{trans}$, which avoids the mechanical impact and improves the stability of the detector operation.

The shape memory mechanism was shown in Fig. 6e. SMP is usually composed of a fixed phase and a reversible phase, among them, the fixed

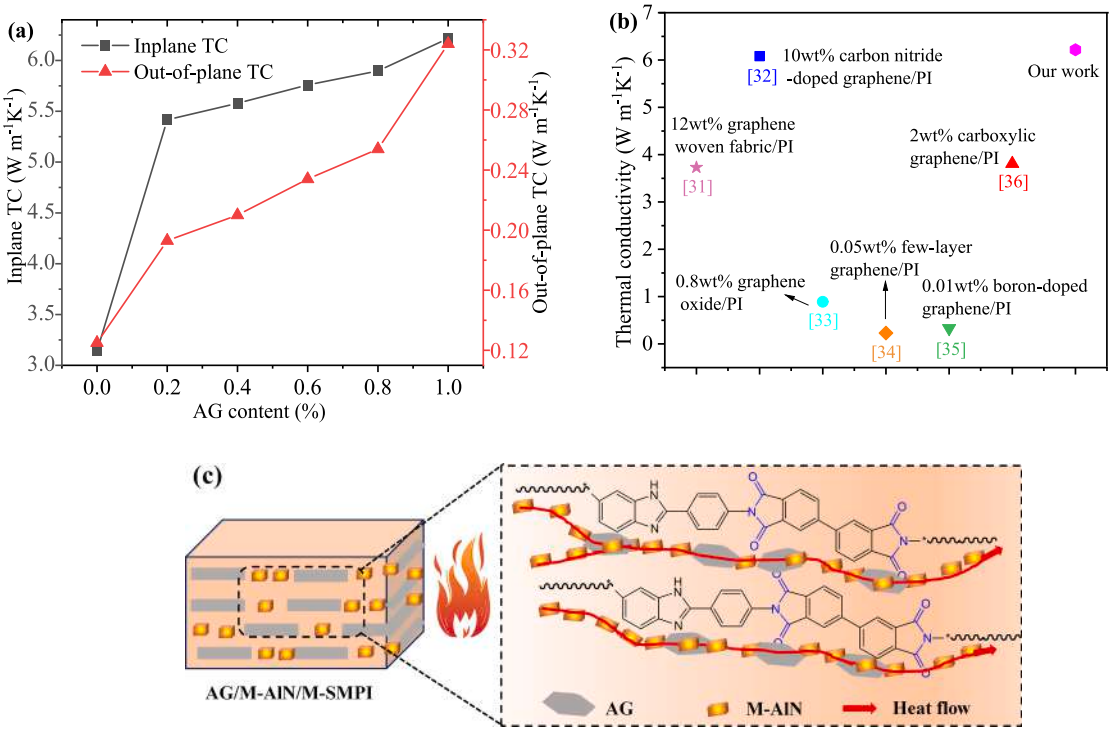


**Fig. 5.** (a) TC of SMPI resin matrix and AG/M-AlN/M-SMPI composites. (b) Comparison of TC with other documents. (c) Diagram of the surface heat dissipation of AG/M-AlN/M-SMPI composite.

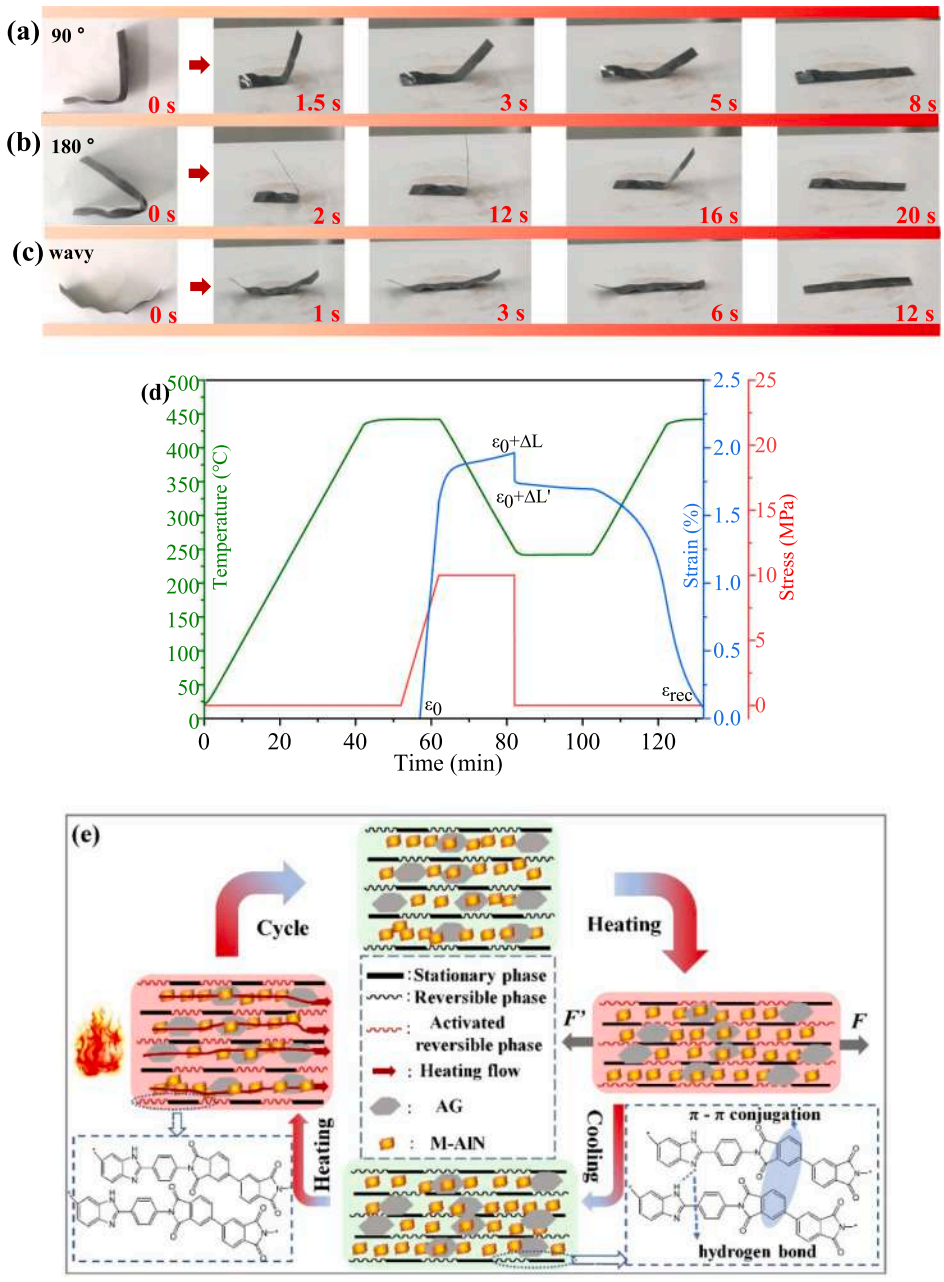


**Fig. 6.** (a–c) Shape recovery processes of the sample bent at 90°, 180°, and wavy shape, respectively. (d) Thermal mechanical cycle processes of AG/M-AlN/M-SMPI-0.8. (e) Schematic diagram of shape memory mechanism of SMPI composite with "spot-plane" directional thermally conduction structures.

phase remembers the initial status of the SMP, while the reversible phase enables the SMP to undergo reversible softening and fixation at different temperatures. For the SMPI, the fixed phase is consisted of strong hydrogen bonding and π-π stacking interactions between imide rings and aromatic rings, while the reversible phase is composed of asymmetric imidazole rings. When the temperature is higher than the $T_{trans}$, the molecular chain of the reversible phase is in a high elasticity state, at the same time, an external force deforms the SMPI to a temporary shape. Then, the SMPI is cooled below the $T_{trans}$, so that the molecular chain segment motion is frozen. After removing the external force, the temporary shape remains unchanged. When the temperature rises to the $T_{trans}$ again, the reversible phase molecular chains are rearranged under the entropy elasticity effect, while the stationary phase still holds solidified status, at the same time, the SMPI returns to the original status, that is, the permanent shape. Based on the previous work [30], AlN nanoparticles could improve the thermal conductivity of SMPI composite, as shown in Supporting Information, Scheme 2. During the shape recovery process, AlN nanoparticles in the SMPI composite film could decline the interfacial phonon scattering and decrease the interfacial thermal resistance between matrix and fillers, thereby enhancing the thermal conduction capability of the SMPI composite and accelerating the heat transfer in the resin matrix. This accelerates the "thawing" of the "frozen" molecular chain segments in the reversible phase, and shortens the response time of the SMPI composite to achieve rapid deformation. Moreover, the two-dimensional acidified graphene has oriented arrangement, which is as the "thermal conductive plane" to increase the thermal conduction connection with AlN nanoparticles and form the "spot-plane" structure, so, the thermal conduction property of the SMPI composite is improved. And the molecular chain segments "thawing" and motion are also accelerated, which realizes rapid shape recovery of the high-$T_g$ SMPI.

## 4. Conclusions

In this paper, we fabricated rapid-response SMPI composites with "spot-plane" directional thermally conduction structures, among them, AlN nanoparticles were as "thermal conduction spots", while acidified graphene was as two-dimensional "thermal conduction planes". Specifically, graphene was acidified to make its surface rich in hydroxyl and carboxyl groups, and directionally arranged under the electric field effect. When the content of M-AlN and acidified graphene were 6 wt% and 0.8 wt%, respectively, the tensile strength of the composite was 134.5 MPa and the Young's modulus was up to 3.80 GPa. and the $T_{trans}$ was 419 ℃, and the shape fixation ratio and shape recovery ratio were 89% and 96%, respectively. Compared with SMPI resin matrix, the response time was shortened by 140 s, only 20 s. Therefore, the problem of long response time of high-$T_g$ SMPI was solved, which had broad applications in flexible electronics, intelligent actuators, and high-temperature active deformation structure, etc.

## CRediT authorship contribution statement

**Xiaofei Wang:** Data curation, Investigation, Methodology, Visualization, Writing – original draft, Writing – review & editing. **Yang He:** Investigation, Methodology, Project administration, Resources, Validation, Writing – review & editing. **Xinli Xiao:** Project administration, Resources, Validation, Writing – review & editing. **Wei Zhao:** Investigation, Methodology, Validation, Writing – review & editing. **Jinsong Leng:** Conceptualization, Funding acquisition, Project administration, Supervision, Writing – review & editing.

## Declaration of Competing Interest

The authors declare that they have no known competing financial interests or personal relationships that could have appeared to influence the work reported in this paper.

## Data availability

Data will be made available on request.

## Acknowledgements

This work was supported by the National Key R&D Program of China (No.2022YFB3805700), National Natural Science Foundation of China (No.92271206), and Science Foundation of National Key Laboratory of Science and Technology on Advanced Composites in Special Environments (No. 6142905222910).

## Appendix A. Supplementary material

Supplementary data to this article can be found online at https://doi.org/10.1016/j.compstruct.2023.117846.

## References

[1] Xu LD, Zhao JT, Shi MF, Liu JB, Wang ZQ. Thermodynamic properties of TPI shape memory polymer composites reinforced by GO/$SiO_2$ modified carbon fiber. Compos Sci Technol 2022;226:109551. https://doi.org/10.1016/j.compscitech.2022.109551.
[2] Zhao W, Li N, Liu LW, Leng JS, Liu YJ. Mechanical behaviors and applications of shape memory polymer and its composites. Appl Phys Rev 2023;10(1):11306. https://doi.org/10.1063/5.0126892.
[3] Zhao W, Zhu J, Liu LW, Leng JS, Liu. Y.J. A bio-inspired 3D metamaterials with chirality and anti-chirality topology fabricated by 4D printing. Int J Smart Nano Mater 2023;14(1):1–20. https://doi.org/10.1080/19475411.2022.2120110.
[4] Yang Y, Wang YQ, Yao T, Feng XJ. A flexible and smart shape memory alloy composite sheet based on efficient and bidirectional thermal management. Int J Smart Nano Mater 2022;13(2):315–29. https://doi.org/10.1080/19475411.2022.2076754.
[5] Zeng CJ, Liu LW, Du Y, Yu M, Xin XZ, Liu TZ, et al. A shape-memory deployable subsystem with a large folding ratio in China's Tianwen-1 Mars exploration mission. Engineering 2023;28:52–60. https://doi.org/10.1016/j.eng.2023.01.005.
[6] Sun WJ, Liang HW, Zhang F, Li B. Theoretical study of the electroactive bistable actuator and regulation methods. Int J Smart Nano Mater 2022;14(1):36–56. https://doi.org/10.1080/19475411.2022.2152128.
[7] Shi S, Cui M, Sun FX, Zhu KK, Lqbal ML, Chen XY, et al. An innovation solvent-responsive coiling-expanding stent. Adv Mater 2021;33:2101005. https://doi.org/10.1002/adma.202101005.
[8] Hu JL, Zhu T, Huang HH, Lu J. Recent advances in shape–memory polymers: structure, mechanism, functionality, modeling and applications. Prog Polym Sci 2012;37:1720–63. https://doi.org/10.1016/j.progpolymsci.2012.06.001.
[9] Davidson JD, Goulbourne NC. Microscopic mechanisms of the shape memory effect in crosslinked polymers. Smart Mater Struct 2015;24(5):055014. https://doi.org/10.1088/0964-1726/24/5/055014.
[10] Yang ZH, Zhang YM, Li S, Zhang XR, Wang TM, Wang QH. Fully closed-loop recyclable thermosetting shape memory polyimide. ACS Sustainable Chem Eng 2020;8(51):18869–78. https://doi.org/10.1021/acssuschemeng.0c05481.
[11] Yang ZT, Yang Z, Zeng JJ, Yang JX, Cao XW. Preparation and properties of biodegradable shape memory polylactic acid/poly(epsilon-caprolactone) blends under volume elongational deformation. Macromol Mater Eng 2022;308(1):2200342. https://doi.org/10.1002/mame.202200342.
[12] Prajapati S, Gogoi R, Tyagi VK, Talwar M, Kumar M, Chaudhari CV. Effect of gamma irradiation on shape memory, thermal and mechanical properties of polycaprolactone. Radiat Phys Chem 2023;204:110671. https://doi.org/10.1016/j.radphyschem.2022.110671.
[13] Hsu WH, Lin CW, Chen YH, Wu SR, Tsai HY. Study on carbon nanotube/shape memory polymer composites and their applications in wireless worm actuator. J Mech 2022;37:636–50. https://doi.org/10.1093/jom/ufab029.
[14] Yao J, Ma S, Zhang J, Wang Y, Wang C, Zhou H, et al. Multiple shape memory effects of polyimide nanocomposites based on octa(aminophenyl) silsequioxanes. Express Polym Lett 2021;15(5):433–44. https://doi.org/10.3144/expresspolymlett.2021.37.
[15] Tan W, Lv JB, Li RK, Hu JH, Zeng K, Yang G. Bio-based adenine-containing copolyimides with high switching temperatures and high-strain storage. Mol Syst Des Eng 2022;7(8):986–95. https://doi.org/10.1039/d2me00031h.
[16] Feng CP, Ni HY, Chen J, Yang W. Facile method to fabricate highly thermally conductive graphite/PP composite with network structures. ACS Appl Mater Interfaces 2016;8(30):19732–8. https://doi.org/10.1021/acsami.6b03723.
[17] Bard S, Demleitner M, Radtke M, Altstadt V. Transverse thermal conductivity of epoxy carbon fiber prepreg laminates with a graphite filled matrix. Compos Sci Technol 2019;3(2):44. https://doi.org/10.3390/jcs3020044.
[18] Ao XL, Kong DY, Zhang ZY, Xiao XL. Enhancing recovery speed and anti-wear capability of high-temperature shape memory polymer with modified boron nitride nanoparticles. J Mater Sci 2020;55(10):4292–302. https://doi.org/10.1007/s10853-019-04319-5.
[19] Xiao M, Du BX. Review of high thermal conductivity polymer dielectrics for electrical insulation. High Volt 2016;1(1):34–42. https://doi.org/10.1049/hve.2016.0008.
[20] Xu YS, Chung DDL. Increasing the thermal conductivity of boron nitride and aluminum nitride particle epoxy-matrix composites by particle surface treatments. Compos Interf 2012;7(4):243–56. https://doi.org/10.1163/156855400750244969.
[21] Huang XY, Jiang PK, Tanaka T. A review of dielectric polymer composites with high thermal conductivity. IEEE Electr Insul M 2011;27(4):8–16. https://doi.org/10.1109/MEI.2011.5954064.
[22] Peng WY, Huang XY, Yu JH, Jiang PK, Liu WH. Electrical and thermophysical properties of epoxy/aluminum nitride nanocomposites: effects of nanoparticle surface modification. Compos Part A-Appl S 2010;41(9):1201–9. https://doi.org/10.1016/j.compositesa.2010.05.002.
[23] Zhao YJ, He JH. Novel template-assisted microwave conversion of graphene oxide to graphene patterns: a reduction transfer mechanism. Carbon 2019;148:159–63. https://doi.org/10.1016/j.carbon.2019.03.081.
[24] Ding JH, Shi S, Zhao HR, Liu PL, Yu HB. Graphdiyne-based thermal fluids. Carbon 2021;176:235–41. https://doi.org/10.1016/j.carbon.2021.01.118.
[25] Zhang K, Tang X, Guo FZ, Xiao KL, Zheng DX, Ma YS, et al. Improved dynamic compressive and electro-thermal properties of hybrid nanocomposite visa physical modification. Nanomaterials 2023;13(1):52. https://doi.org/10.3390/nano13010052.
[26] Wang Y, Li SS, Yang HY, Luo J. Progress in the functional modification of graphene/graphene oxide: A review. RSC Adv 2020;10(26):15328–45. https://doi.org/10.1039/d0ra01068e.
[27] Ahmed MS, Begum H, Kim YB, Jung S. Surface functionalization of acidified graphene through amidation for enhanced oxygen reduction reaction. Appl Surf Sci 2021;536:147760. https://doi.org/10.1016/j.apsusc.2020.147760.
[28] Arenas-Guerrero P, Delgado AV, Jimenez ML. Analysis of the electro-optical response of graphene oxide dispersions under alternating fields. Carbon 2018;144:395–401. https://doi.org/10.1016/j.carbon.2018.12.046.
[29] Kuznetsova A, Popova I, Yates JT, Bronikowski MJ, Huffman CB, Liu J, et al. Oxygen-containing functional groups on single-wall carbon nanotubes: NEXAFS and vibrational spectroscopic studies. J Am Chem Soc 2001;123(43):10699–704. https://doi.org/10.1021/ja011021b.
[30] Wang XF, He Y, Xiao XL, Leng JS. Rapid thermal-actuated ultrahigh $T_g$ shape memory polyimide composites with "micro-nano" particle synergistic effect. Compos Sci Technol 2023;239:110052. https://doi.org/10.1016/j.compscitech.2023.110052.

[31] Gong JR, Liu ZD, Yu JH, Dai D, Dai W, Du SY, et al. Graphene woven fabric-reinforced polyimide films with enhanced and anisotropic thermal conductivity. Compos Part A-Appl S 2016;87:290–6. https://doi.org/10.1016/j.compositesa.2016.05.010.
[32] Wang YY, Zhang X, Ding X, Li Y, Zhang P, Shu MT, et al. Enhanced thermal conductivity of carbon nitride-doped graphene/polyimide composite film via a "deciduous-like" strategy. Compos Sci Technol 2021;205:108693. https://doi.org/10.1016/j.compscitech.2021.108693.
[33] Fazil S, Saeed S, Waseem M, Rehman W, Bangesh M, Liaqat K. Improving mechanical, thermal, and electrical properties of polyimide by incorporating vinyltriethoxysilane functionalized graphene oxide. Polym Compos 2018;39:E1635–42. https://doi.org/10.1002/pc.24581.
[34] Wang RB, Chen ML, Li Q, Li WW, Guo YF, Liu LW. Enhanced mechanical and thermal properties of polyimide films based on functional groups-free few-layer graphene. J Chem Eng 2019;52(6):570–8. https://doi.org/10.1252/jcej.18we106.
[35] Ha YM, Kim YN, Kim YO, So C, Lee JS, Kim J, et al. Enhanced mechanical properties and thermal conductivity of polyimide nanocomposites incorporating individualized boron-doped graphene. Carbon Lett 2019;30(4):457–64. https://doi.org/10.1007/s42823-019-00115-y.
[36] Ma LR, Wang YX, Xu XD, Wang YY, Wang CG. Structural evolution and thermal conductivity of flexible graphite films prepared by carboxylic graphene/polyimide. Ceram Int 2020;47(1):1076–85. https://doi.org/10.1016/j.ceramint.2020.08.223.
[37] Sun JJ, Yao YM, Zeng XL, Pan GR, Hu JT, Huang Y, et al. Preparation of boron nitride nanosheet/nanofibrillated cellulose nanocomposites with ultrahigh thermal conductivity via engineering interfacial thermal resistance. Adv Mater Interfaces 2017;4(17):1700563. https://doi.org/10.1002/admi.201700563.
[38] Wang XF, He Y, Leng JS. Shape memory polyimides and composites with tunable chain stiffness and ultrahigh transition temperature range. Compos Part A-Appl S 2022;163:107237. https://doi.org/10.1016/j.compositesa.2022.107237.